Hindawi Publishing Corporation
Mathematical Problems in Engineering
Volume 2011, Article ID 208426, 19 pages
doi:10.1155/2011/208426

Research Article

Numerical Investigation into CO_2 Emission, O_2 Depletion, and Thermal Decomposition in a Reacting Slab

O. D. Makinde,[1] T. Chinyoka,[2] and R. S. Lebelo[1]

[1] *Institute for Advance Research in Mathematical Modeling and Computations, Cape Peninsula University of Technology, P.O. Box 1906, Bellville 7535, South Africa*
[2] *Center for Research in Computational and Applied Mechanics, University of Cape Town, Rondebosch 7701, South Africa*

Correspondence should be addressed to T. Chinyoka, tchinyok@vt.edu

Received 29 January 2011; Revised 15 June 2011; Accepted 25 July 2011

Academic Editor: Ben T. Nohara

The emission of carbon dioxide (CO_2) is closely associated with oxygen (O_2) depletion, and thermal decomposition in a reacting stockpile of combustible materials like fossil fuels (e.g., coal, oil, and natural gas). Moreover, it is understood that proper assessment of the emission levels provides a crucial reference point for other assessment tools like climate change indicators and mitigation strategies. In this paper, a nonlinear mathematical model for estimating the CO_2 emission, O_2 depletion, and thermal stability of a reacting slab is presented and tackled numerically using a semi-implicit finite-difference scheme. It is assumed that the slab surface is subjected to a symmetrical convective heat and mass exchange with the ambient. Both numerical and graphical results are presented and discussed quantitatively with respect to various parameters embedded in the problem.

1. Introduction

Studies relating to transient heating of combustible materials due to exothermic oxidation chemical reactions are extremely important and have a wide range of applications in industry, engineering, and environmental science [1]. For instance, fossil fuels (coal, oil, and natural gas) account for 85% of world's primary energy supply, 70% of worlds electricity and heat generation and over 94% of energy for transportation [2]. The production and use of these combustible materials contribute up to 80% of CO_2 emission. Given expected increases in global population, economic growth, and energy demand, a continuous rise in emissions is expected unless fundamental technology changes occur in global energy systems which

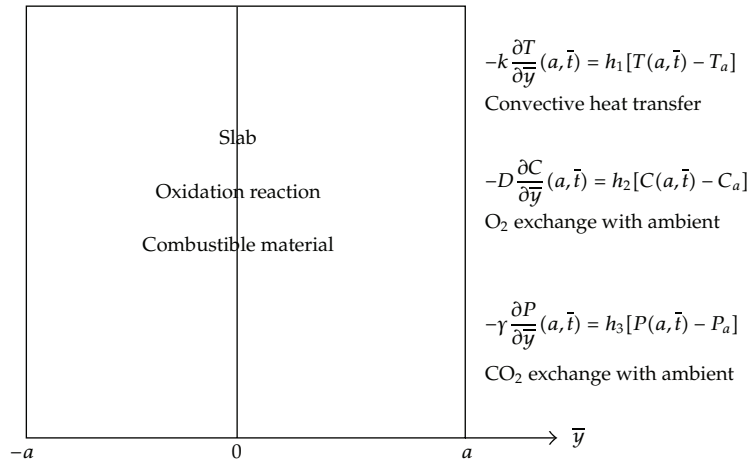

Figure 1: Geometry of the problem.

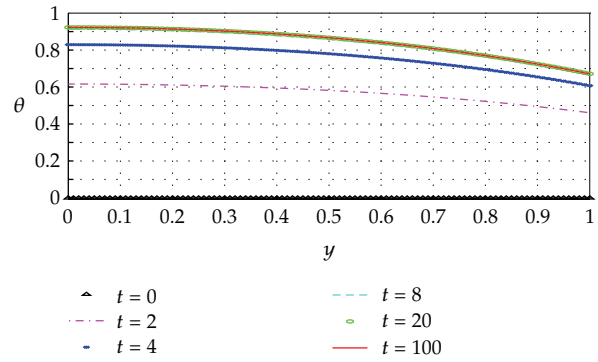

Figure 2: Transient and steady-state temperature profiles.

are currently dominated by fossil fuels. The CO_2 pollution is the principal human cause of global warming and climate change [3]. Meanwhile, for proper assessment of the CO_2 emission and O_2 depletion levels together with their impact on both the environment and life on Earth, knowledge of the mathematical models of these complex chemical systems is essential. These provide crucial reference points for other assessment tools like thermal stability of the materials, climate change indicators, and mitigation strategies. It may also help in developing medium to long-term action plans for climate change research and reliable design of the systems [4].

An extensive review of detailed chemical kinetic models for the heating-up of combustible materials is given by Simmie [5]. His review considered post-1994 work and focuses on the modeling of hydrocarbon fuel oxidation in the gas phase by detailed chemical kinetics and those experiments which validate them. Moreover, thermal combustion analysis has received much attention in the literature [6–8]. Several studies have been directed towards obtaining critical conditions for thermal ignition to occur in the form of a critical value for the Frank-Kamenetskii parameter [9]. Usually, chemical processes include many, up to a several hundred, intermediate elementary reactions [10]. For example, in

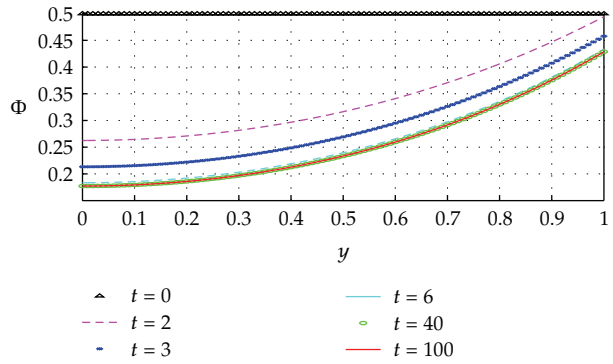

Figure 3: Transient and steady state oxygen profiles.

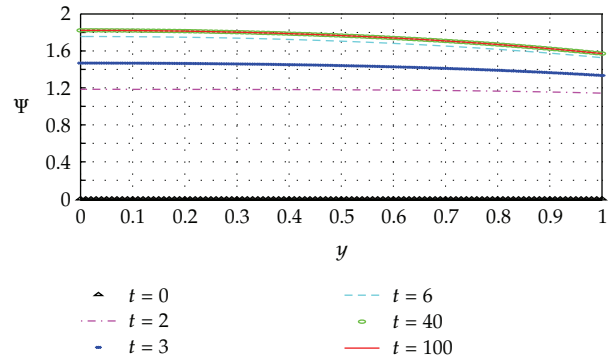

Figure 4: Transient and steady state carbon dioxide profiles.

combustion science, it is very common to use complex multistep reaction mechanisms to predict the oxidation of hydrocarbons [11]. However, the use of one-step decomposition kinetics clearly simplifies the complicated chemistry involved in the problem but is both practical and necessary without additional information about the individual decomposition reaction steps [12, 13]. Meanwhile, analytical solutions of the partial differential equations governing transient heating of the combustible material undergoing oxidation reactions are usually impossible or extremely difficult to obtain. The exothermic nature of such reactions leads to complex nonlinear transient interaction of heat conduction, mass diffusion, and chemical reactions, resulting in steep concentration and temperature gradients [14]. In such circumstances, a better understanding of the system behavior can only be accomplished by conducting numerical simulations to capture the frontal behavior of the processes.

The basic objective of this study is to provide a numerical estimate for the thermal stability together with the rate of CO_2 emission and O_2 depletion in transient heating of a slab of combustible material in the presence of convective heat and mass exchange with the ambient at the slab surface. The mathematical formulation of the problem is established in section two. In section three, the semi-implicit finite difference technique is implemented to tackle the problem. Both numerical and graphical results are presented and discussed quantitatively with respect to various parameters embedded in the system in Section 4.

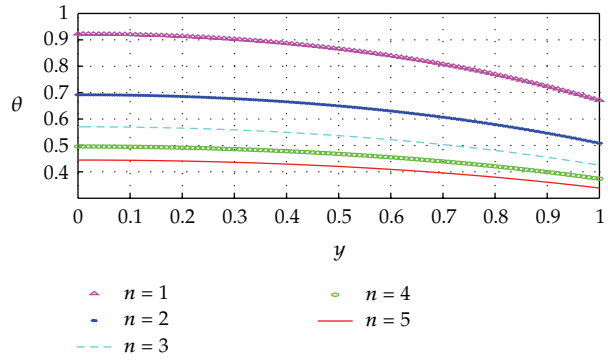

Figure 5: Effects of n on temperature.

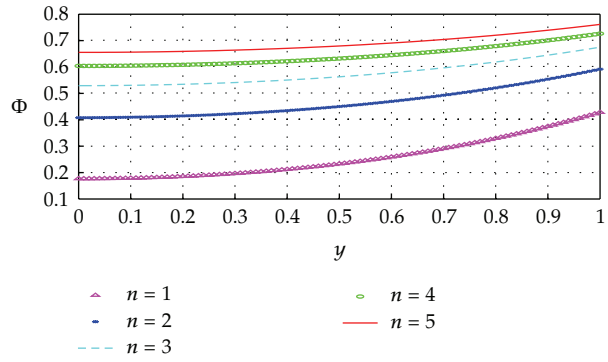

Figure 6: Effects of n on O_2.

2. Mathematical Model

We consider a stockpile of combustible material in a rectangular slab. It is assumed that the slab is undergoing an nth-order oxidation chemical reaction, and its surface is subjected to a symmetrical convective heat and mass exchange with the ambient (see Figure 1). The complicated chemistry involved in this problem can be simplified by assuming a one-step finite-rate irreversible reaction between the combustible material (hydrocarbon) and the oxygen of the air; that is,

$$C_iH_j + \left(i + \frac{j}{4}\right)O_2 \longrightarrow iCO_2 + \frac{j}{2}H_2O + \text{Heat}. \tag{2.1}$$

Following [1, 5, 6, 12, 14], the nonlinear partial differential equations describing temperature, oxygen, and carbon dioxide concentration in the combustible material can be written as

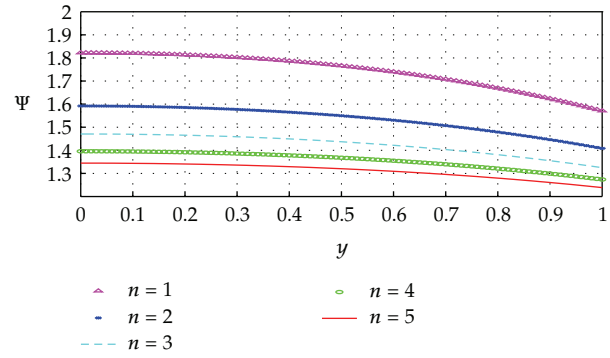

Figure 7: Effects of n on CO_2.

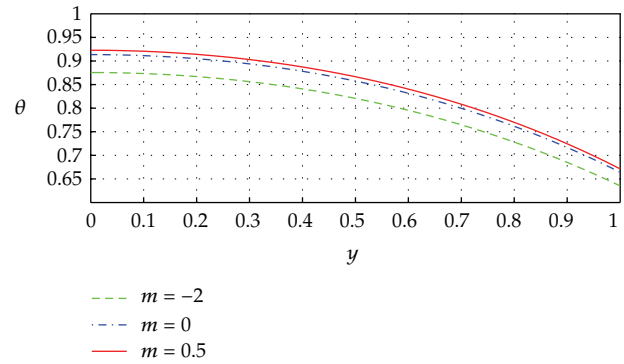

Figure 8: Effects of m on temperature.

$$\rho c_p \frac{\partial T}{\partial \bar{t}} = k\frac{\partial^2 T}{\partial \bar{y}^2} + QA\left(\frac{KT}{\nu l}\right)^m C^n \exp\left(-\frac{E}{RT}\right),$$
$$\frac{\partial C}{\partial \bar{t}} = D\frac{\partial^2 C}{\partial \bar{y}^2} - A\left(\frac{KT}{\nu l}\right)^m C^n \exp\left(-\frac{E}{RT}\right), \tag{2.2}$$
$$\frac{\partial P}{\partial \bar{t}} = \gamma\frac{\partial^2 P}{\partial \bar{y}^2} + A\left(\frac{KT}{\nu l}\right)^m C^n \exp\left(-\frac{E}{RT}\right),$$

with initial and boundary conditions as follows:

$$T(\bar{y},0) = T_0, \qquad C(\bar{y},0) = \frac{1}{2}C_a, \qquad P(\bar{y},0) = 0,$$
$$\frac{\partial T}{\partial \bar{y}}\left(0,\bar{t}\right) = \frac{\partial C}{\partial \bar{y}}\left(0,\bar{t}\right) = \frac{\partial P}{\partial \bar{y}}\left(0,\bar{t}\right) = 0,$$
$$-k\frac{\partial T}{\partial \bar{y}}\left(a,\bar{t}\right) = h_1\left[T\left(a,\bar{t}\right) - T_a\right],$$

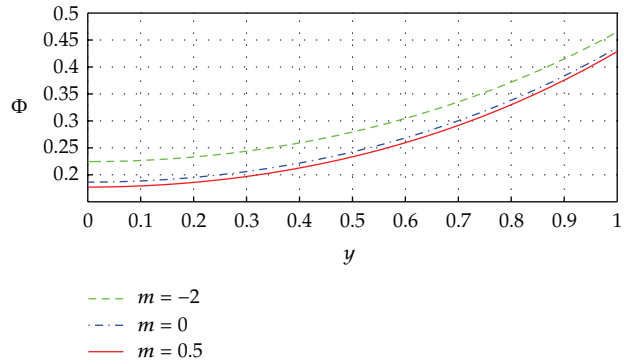

Figure 9: Effects of m on O_2.

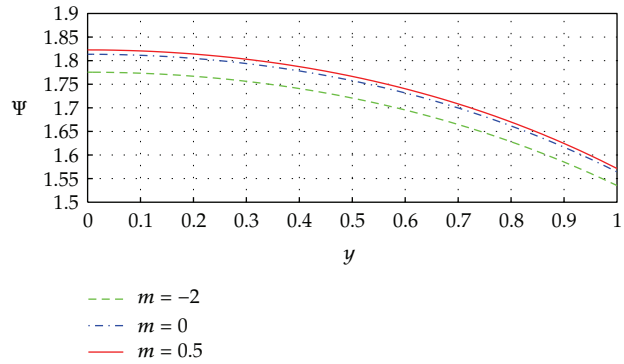

Figure 10: Effects of m on CO_2.

$$-D\frac{\partial C}{\partial \overline{y}}\left(a,\bar{t}\right) = h_2\left[C\left(a,\bar{t}\right) - C_a\right],$$
$$-\gamma\frac{\partial P}{\partial \overline{y}}\left(a,\bar{t}\right) = h_3\left[P\left(a,\bar{t}\right) - P_a\right], \tag{2.3}$$

where T is the absolute temperature, C is the (depletion) oxygen concentration, P is the carbon dioxide emission concentration, T_a is the ambient temperature, C_a is the oxygen concentration in the surrounding air, P_a is the carbon dioxide concentration in the surrounding air, $\bar{t}$ is the time, T_0 is the slab initial temperature, the initial depletion of oxygen in the slab is zero, ρ is the density, c_p specific heat at constant pressure, k is the thermal conductivity of the reacting slab, D is the diffusivity of oxygen in the slab, γ is the diffusivity of carbon dioxide in the slab, Q is the exothermicity, A is the rate constant, E is the activation energy, R is the universal gas constant, l is the Planck number, K is the Boltzmann constant, ν is the vibration frequency, a is the slab half width, $\overline{y}$ is the distance measured transverse direction, h_1 is the coefficient of heat transfer between the slab and its surroundings, h_2 is the coefficient of oxygen transfer between the slab and its surroundings, h_3 is the coefficient of carbon dioxide transfer between the slab and its surroundings, n is the order of exothermic

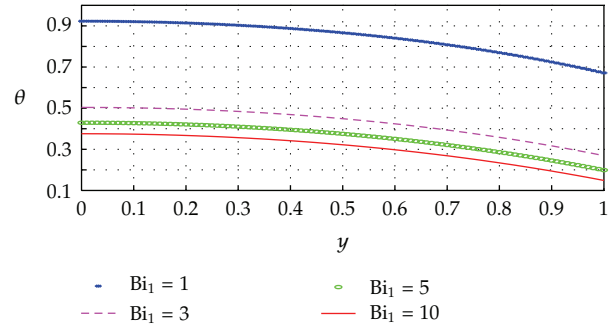

Figure 11: Effects of Bi_1 on temperature.

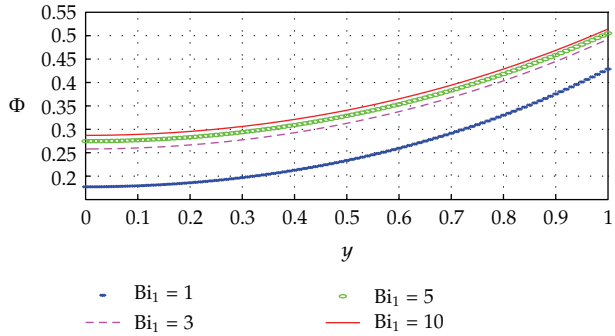

Figure 12: Effects of Bi_1 on O_2.

chemical reaction, and m is the numerical exponent such that $m \in \{-2, 0, 0.5\}$. The three values taken by the parameter m represent the numerical exponent for sensitized, Arrhenius and Bimolecular kinetics, respectively, (see [1, 6]). We introduce the following dimensionless variables into (2.2)-(2.3):

$$\theta = \frac{E(T-T_0)}{RT_0^2}, \quad \theta_a = \frac{E(T_a-T_0)}{RT_0^2}, \quad \Phi = \frac{C}{C_a}, \quad \Psi = \frac{P}{P_a},$$
$$\mathrm{Bi}_1 = \frac{ah_1}{k}, \quad \mathrm{Bi}_2 = \frac{ah_2}{D}, \quad \mathrm{Bi}_3 = \frac{ah_2}{\gamma}, \quad \beta_1 = \frac{\rho c_p RT_0^2}{QEC_a},$$
$$\beta_2 = \frac{\rho c_p RT_0^2}{QEP_a}, \quad \lambda = \left(\frac{KT_0}{\nu l}\right)^m \frac{QAEa^2C_a^n}{kRT_0^2} \exp\left(-\frac{E}{RT}\right), \tag{2.4}$$
$$y = \frac{\overline{y}}{a}, \quad t = \frac{k\bar{t}}{\rho c_p a^2}, \quad \varepsilon = \frac{RT_0}{E}, \quad \alpha = \frac{D\rho c_p}{k}, \quad \sigma = \frac{\gamma \rho c_p}{k},$$

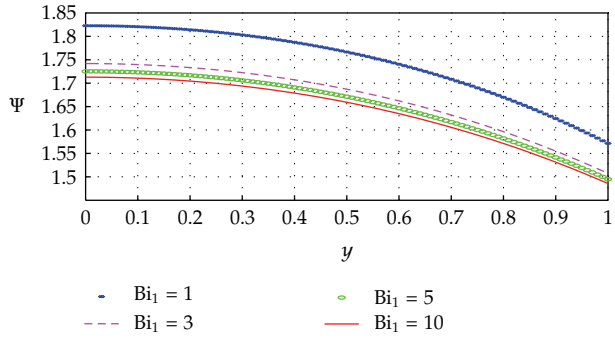

Figure 13: Effects of Bi_1 on CO_2.

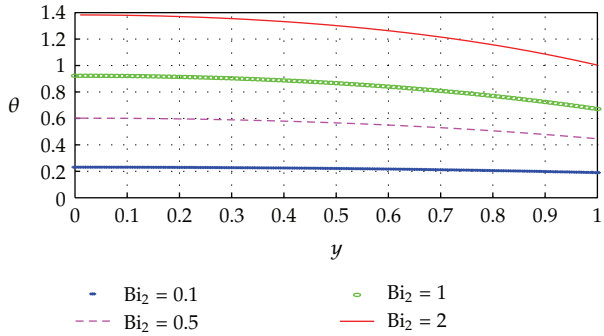

Figure 14: Effects of Bi_2 on temperature.

and we obtain the dimensionless governing equations as

$$\begin{aligned}
\frac{\partial\theta}{\partial t} &= \frac{\partial^2\theta}{\partial y^2} + \lambda(1+\varepsilon\theta)^m\Phi^n \exp\left(\frac{\theta}{1+\varepsilon\theta}\right),\\
\frac{\partial\Phi}{\partial t} &= \alpha\ \frac{\partial^2\Phi}{\partial y^2} - \lambda\beta_1(1+\varepsilon\theta)^m\ \Phi^n \exp\left(\frac{\theta}{1+\varepsilon\theta}\right),\\
\frac{\partial\Psi}{\partial t} &= \sigma\ \frac{\partial^2\Psi}{\partial y^2} + \lambda\beta_2(1+\varepsilon\theta)^m\ \Phi^n \exp\left(\frac{\theta}{1+\varepsilon\theta}\right).
\end{aligned} \tag{2.5}$$

The corresponding initial and boundary conditions then become

$$\begin{gathered}
\theta(y,0) = 0, \qquad \Phi(y,0) = 0.5, \qquad \Psi(y,0) = 0,\\
\frac{\partial\theta}{\partial y}(0,t) = \frac{\partial\Phi}{\partial y}(0,t) = \frac{\partial\Psi}{\partial y}(0,t) = 0,\\
\frac{\partial\theta}{\partial y}(1,t) = -\mathrm{Bi}_1[\theta(1,t) - \theta_a],
\end{gathered}$$

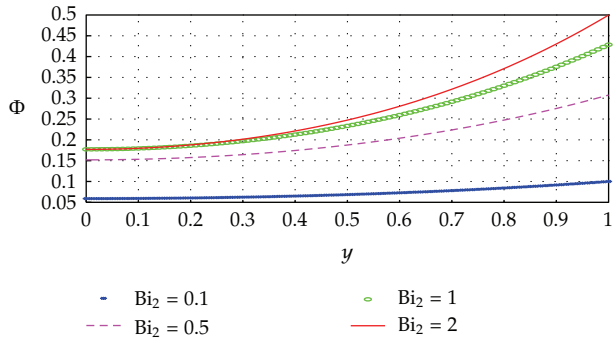

Figure 15: Effects of Bi_2 on O_2.

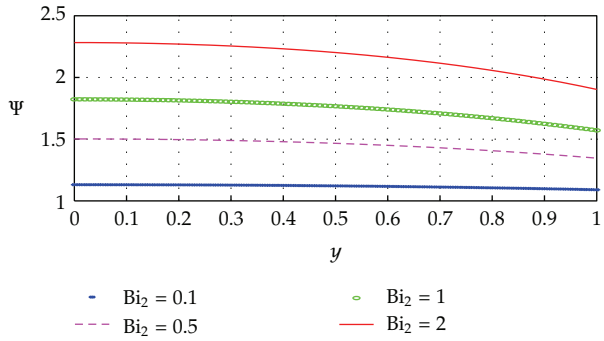

Figure 16: Effects of Bi_2 on CO_2.

$$\frac{\partial \Phi}{\partial y}(1,t) = -\mathrm{Bi}_2[\Phi(1,t) - 1],$$
$$\frac{\partial \Psi}{\partial y}(1,t) = -\mathrm{Bi}_3[\Psi(1,t) - 1], \tag{2.6}$$

where λ, ε, β_1, β_2, α, σ, Bi_1, Bi_2, and Bi_3 represent the Frank-Kamenetskii parameter, activation energy parameter, oxygen consumption rate parameter, carbon dioxide emission rate parameter, oxygen diffusivity parameter, carbon dioxide diffusivity parameter, the thermal Biot number, oxygen Biot number, and carbon dioxide Biot number, respectively. A body of material releasing heat to its surroundings may achieve a safe steady state where the temperature of the body reaches some moderate value and stabilizes. However, when the rate of heat generation in the material exceeds the rate of heat loss to the surroundings, then ignition can occur. In the following sections, (2.5)-(2) are solved numerically using a semi-implicit finite difference scheme.

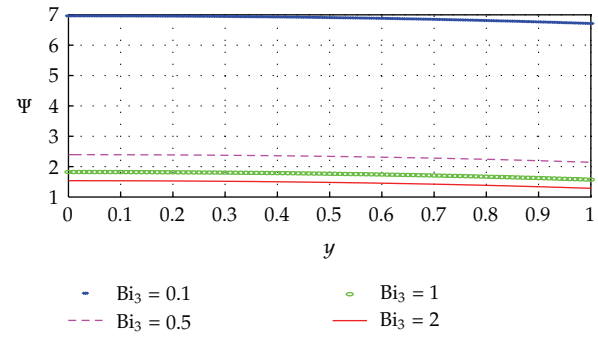

Figure 17: Effects of Bi_3 on CO_2.

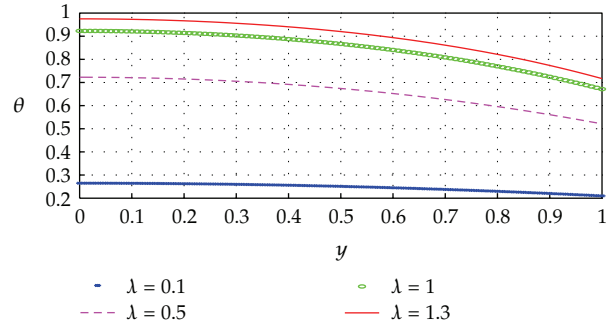

Figure 18: Effects of λ on temperature.

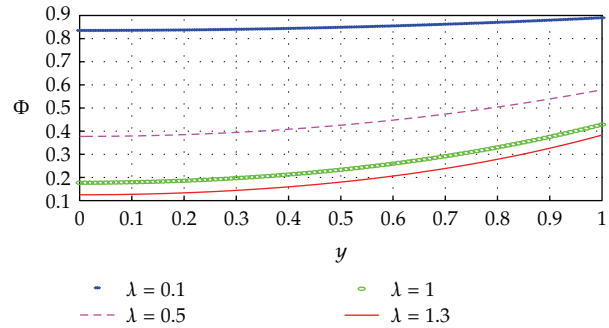

Figure 19: Effects of λ on O_2.

3. Numerical Solution

Our numerical algorithm is based on the semi-implicit finite difference scheme [15–18]. The implicit terms are taken at the intermediate time level $(N + \xi)$ where $0 \leq \xi \leq 1$. The algorithm employed in [18] uses $\xi = 1/2$, we will, however, follow the formulation in [15–17] and take $\xi = 1$ in this paper so that we can use larger time steps. In fact being nearly fully implicit, our numerical algorithm presented in this paper is conjectured to work for any value of the time step! The discretization of the governing equations is based on a linear Cartesian mesh and uniform grid on which finite differences are taken. We approximate both the second and first spatial derivatives with second-order central differences. The equations corresponding to

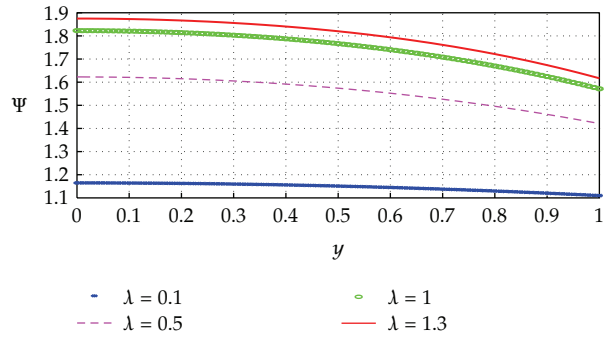

Figure 20: Effects of λ on CO_2.

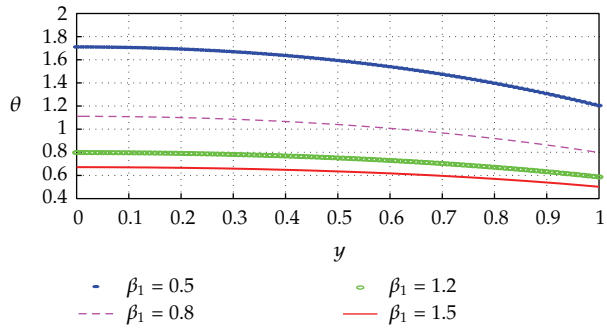

Figure 21: Effects of β_1 on temperature.

the first and last grid points are modified to incorporate the boundary conditions. The semi-implicit schemes for the temperature, O_2 concentration, and CO_2 concentration, respectively, read

$$\frac{\theta^{(N+1)}-\theta^{(N)}}{\Delta t}=\frac{\partial^2}{\partial y^2}\theta^{(N+\xi)}+\lambda\left[(1+\varepsilon\theta)^m\Phi^n\exp\left(\frac{\theta}{1+\varepsilon\theta}\right)\right]^{(N)},$$

$$\frac{\Phi^{(N+1)}-\Phi^{(N)}}{\Delta t}=\alpha\frac{\partial^2}{\partial y^2}\Phi^{(N+\xi)}-\lambda\beta_1\left[(1+\varepsilon\theta)^m\Phi^n\exp\left(\frac{\theta}{1+\varepsilon\theta}\right)\right]^{(N)},$$

$$\frac{\Psi^{(N+1)}-\Psi^{(N)}}{\Delta t}=\sigma\frac{\partial^2}{\partial y^2}\Psi^{(N+\xi)}+\lambda\beta_2\left[(1+\varepsilon\theta)^m\Phi^n\exp\left(\frac{\theta}{1+\varepsilon\theta}\right)\right]^{(N)}. \tag{3.1}$$

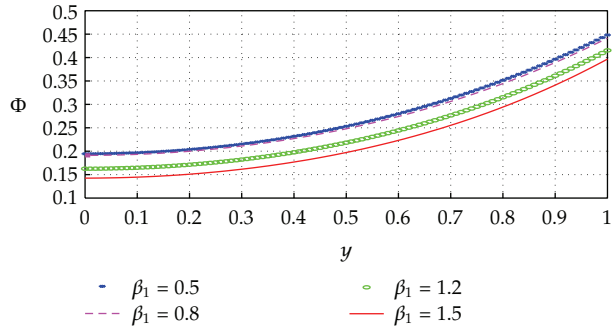

Figure 22: Effects of β_1 on O_2.

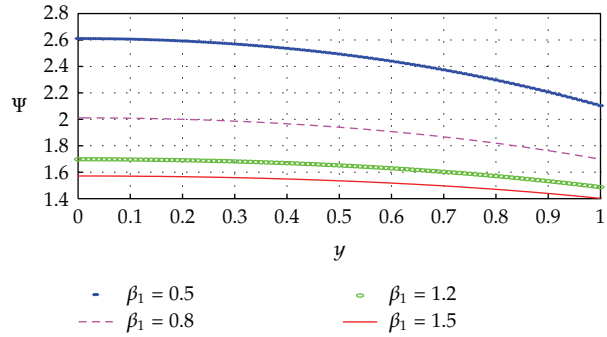

Figure 23: Effects of β_1 on CO_2.

The equations for $\theta^{(N+1)}$, $\Phi^{(N+1)}$, and $\Psi^{(N+1)}$, thus, become

$$\begin{aligned}
-r\xi\theta_{j-1}^{(N+1)} + (1+2r\xi)\theta_j^{(N+1)} - r\xi\theta_{j+1}^{(N+1)} &= -r(1-\xi)\theta_{j-1}^{(N)} + (1-2r(1-\xi))\theta_j^{(N)} \\
&\quad - r(1-\xi)\theta_{j+1}^{(N)} \\
&\quad + \lambda\Delta t\left[(1+\varepsilon\theta_j)^m\Phi_j^n\exp\left(\frac{\theta_j}{1+\varepsilon\theta_j}\right)\right]^{(N)}, \\
-r\xi\alpha\Phi_{j-1}^{(N+1)} + (1+2r\xi\alpha)\Phi_j^{(N+1)} - r\xi\alpha\Phi_{j+1}^{(N+1)} &= -r(1-\xi)\alpha\Phi_{j-1}^{(N)} + (1-2r(1-\xi)\alpha)\Phi_j^{(N)} \\
&\quad - r(1-\xi)\alpha\Phi_{j+1}^{(N)} \\
&\quad - \lambda\Delta t\beta_1\left[(1+\varepsilon\theta_j)^m\Phi_j^n\exp\left(\frac{\theta_j}{1+\varepsilon\theta_j}\right)\right]^{(N)},
\end{aligned}$$

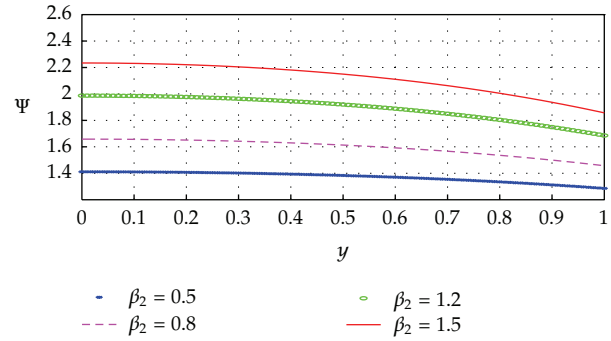

Figure 24: Effects of β_2 on CO_2.

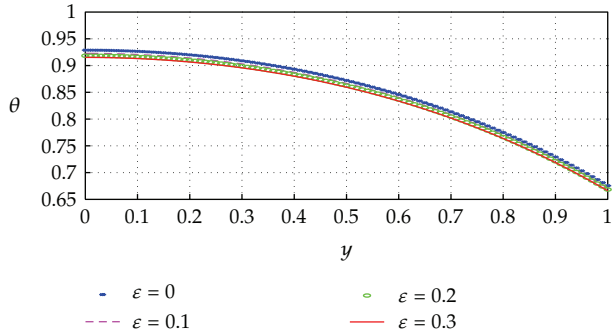

Figure 25: Effects of ε on temperature.

$$-r\xi\sigma\Psi_{j-1}^{(N+1)} + (1+2r\xi\sigma)\Psi_j^{(N+1)} - r\xi\sigma\Psi_{j+1}^{(N+1)} = -r(1-\xi)\sigma\Psi_{j-1}^{(N)} + (1-2r(1-\xi)\sigma)\Psi_j^{(N)} - r(1-\xi)\sigma\Psi_{j+1}^{(N)} + \lambda\Delta t\beta_2\left[(1+\varepsilon\theta_j)^m\Phi_j^n\exp\left(\frac{\theta_j}{1+\varepsilon\theta_j}\right)\right]^{(N)}, \tag{3.2}$$

where $r = \Delta t/\Delta y^2$. The solution procedures reduce to inversion of tridiagonal matrices. The schemes (3.2) were checked for consistency. For $\xi = 1$, these are first-order accurate in time but second order in space. The schemes in [18] have $\xi = 1/2$ which improves the accuracy in time to second order. We use $\xi = 1$ here so that we are free to choose larger time steps and still converge to the steady solutions. As already conjectured, our algorithm works for any value of the time step! The code was checked for both spatial and temporal convergence. In particular, solutions calculated from, say $\Delta t = 1$, using 200 time steps are exactly the same as those after 40 time steps with $\Delta t = 5$ or those after 20,000 time steps with $\Delta t = 0.01$. Similarly solutions using $\Delta y = 0.02$ converge to the same results as those say for $\Delta t = 0.025$ or $\Delta t = 0.05$, and so forth. Our code, thus, runs extremely fast, and; hence, we can easily obtain and, thus, present all our results at steady state using nearly insignificant computational times.

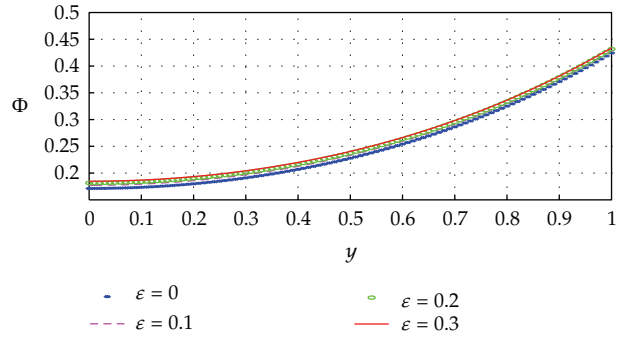

Figure 26: Effects of ε on O_2.

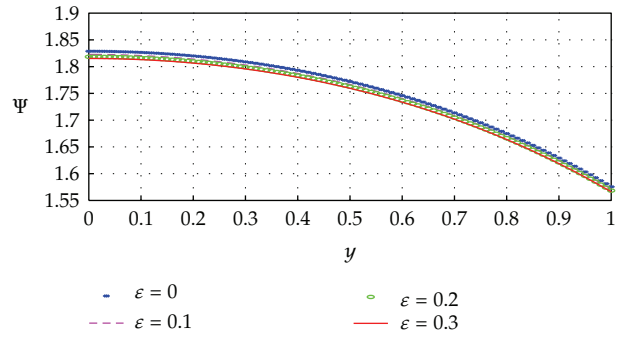

Figure 27: Effects of ε on CO_2.

4. Results and Discussion

Unless otherwise stated, we employ the parameter values:

$$\begin{gathered} m = 0.5, \quad n = 1, \quad \theta_a = 0.1, \quad \alpha = 1, \quad \sigma = 1, \\ \beta_1 = 1, \quad \beta_2 = 1, \quad \mathrm{Bi}_1 = 1, \quad \mathrm{Bi}_2 = 1, \quad \mathrm{Bi}_3 = 1, \\ \varepsilon = 0.1, \quad \Delta y = 0.01, \quad \Delta t = 1, \quad t = 200. \end{gathered} \tag{4.1}$$

These will be the default values in this work, and; hence, in any graph where any of these parameters is not explicitly mentioned, it will be understood that such parameters take on the default values.

4.1. Transient and Steady Flow Profiles

We display the transient solutions in Figures 2, 3, and 4. At the given parameter values, Figure 2 shows a transient increase in temperature until a steady-state is reached. A similar scenario obtains in Figure 4 in which a transient increase of carbon dioxide emission is observed until a steady state is reached. An opposite situation is noticed in Figure 3 where a decrease in oxygen concentration is observed with increasing time until a steady-state

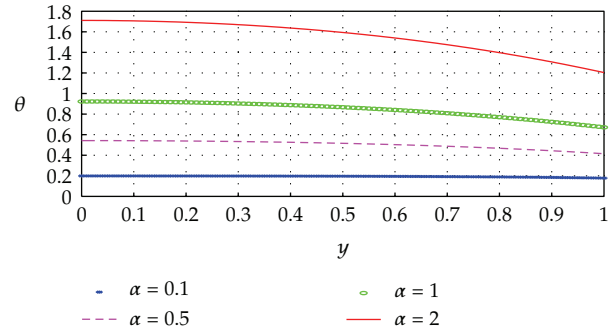

Figure 28: Effects of α on temperature.

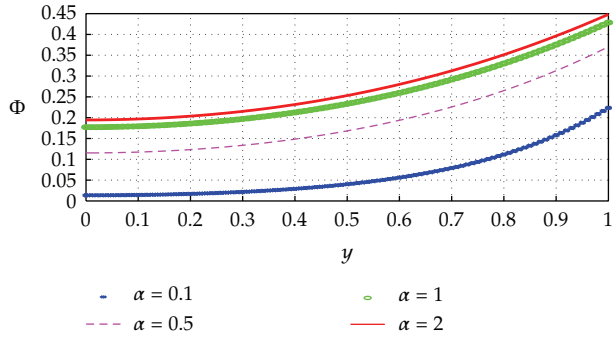

Figure 29: Effects of α on O_2.

concentration is attained. These results are consistent with intuition regarding exothermic oxidation reactions.

4.1.1. Parameter Dependance of Solutions in Steady State

It is understood from Figures 2–4 that, at the default parameter values, solutions have reached steady state at, say, times $t \geq 40$. All the solutions at $t = 200$ given below will, thus, be understood to be steady solutions. The dependence of solutions on parameter n is illustrated in Figures 5, 6, and 7. As n increases, the results show a decrease in both the temperature and the CO_2 emission. The reduced oxidation reactions mean lower oxygen consumption, hence, lead to a corresponding increase in O_2 concentration.

The dependence of solutions on parameter m is illustrated in Figures 8, 9, and 10. As m increases, the results show an increase in both the temperature and the CO_2 emission. The increased oxygen consumption from higher oxidation reactions correspondingly decreases O_2 concentration.

The dependence of solutions on parameter Bi_1 is illustrated in Figures 11, 12, and 13. As Bi_1 increases, the results show a decrease in both the temperature and the CO_2 emission. The reduced oxidation reactions mean lower oxygen consumption, hence, lead to a corresponding increase in O_2 concentration.

The dependence of solutions on parameter Bi_2 is illustrated in Figures 14, 15, and 16. An increase in Bi_2 directly corresponds to an increase in O_2 concentration. This

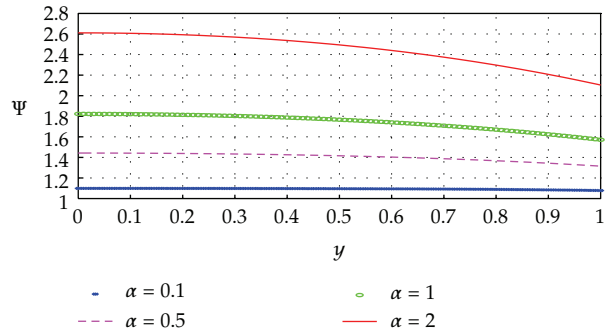

Figure 30: Effects of α on CO_2.

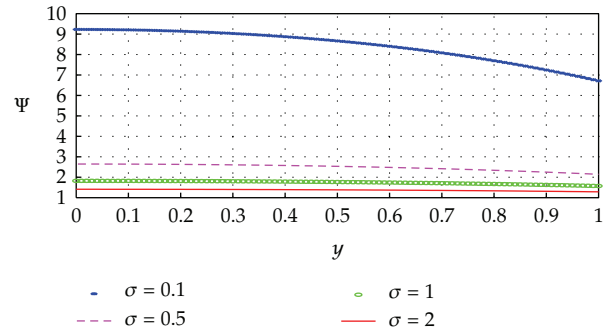

Figure 31: Effects of σ on CO_2.

correspondingly increases the oxidation reactions and, hence, increases the temperature and, hence, the CO_2 emission.

The dependence of CO_2 emission on Bi_3 is shown in Figure 17. An increase in Bi_3 decreases the CO_2 emission. No noticeable effects are observed in the temperature and the O_2 concentration.

The dependence of solutions on the reaction parameter λ is illustrated in Figures 18, 19, and 20. An increase in λ directly corresponds to an increase in the (exothermic) oxidation reactions and, hence, increases the temperature and, hence, the CO_2 emission. The increased oxidation reactions increase oxygen consumption and thus decrease O_2 concentration.

The dependence of solutions on parameter β_1 is shown in Figures 21, 22, and 23. An increase in β_1 directly corresponds to a decrease in O_2 concentration. This correspondingly decreases the oxidation reactions and, hence, decreases the temperature and also CO_2 emission.

The dependence of CO_2 emission on β_2 is shown in Figure 24. An increase in β_2 increases the CO_2 emission. No noticeable effects are observed in the temperature and the O_2 concentration.

The dependence of solutions on the parameter ε is illustrated in Figures 25, 26, and 27. An increase in ε decreases the temperature and the CO_2 emission. The reduced oxygen consumption leads to an increase in O_2 concentration.

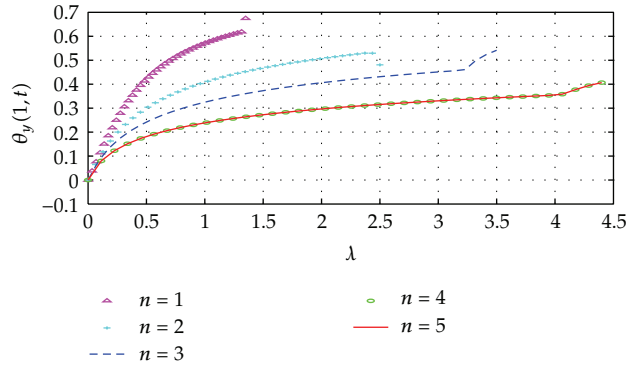

Figure 32: Effects of variation of n on the thermal criticality or blowup in the system.

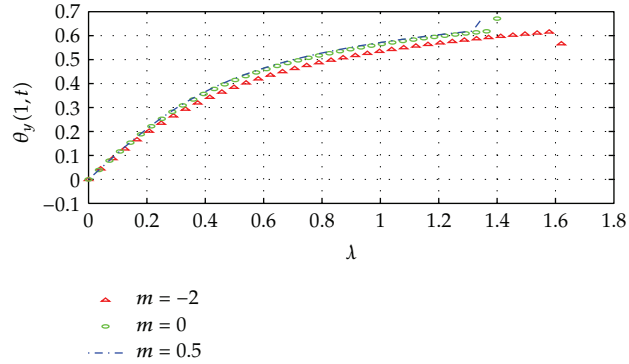

Figure 33: Effects of variation of m on the thermal criticality or blowup in the system.

The dependence of solutions on the parameter α is shown in Figures 28, 29, and 30. An increase in α directly corresponds to an increase in O_2 concentration. This correspondingly increases the oxidation reactions and hence increases the temperature and also CO_2 emission.

The dependence of CO_2 emission on σ is shown in Figure 31. An increase in σ decreases the CO_2 emission. No noticeable effects are observed in the temperature and O_2 concentration.

4.2. Thermal Stability and Blowup

In Figures 32, 33, 34, and 35, we plot $\theta_y(1,t)$ against λ for varying values of n, m, Bi_1, and Bi_2, respectively. The solutions are given up to the values of λ at which the onset of blowup in temperature is observed. We notice that parameters that increase the temperature (θ) correspondingly increase $\theta_y(1,t)$. The results also show that early onset of blowup (and, hence, thermal instability) can be delayed by using higher values of n, lower values of m, higher values of Bi_1, lower values of Bi_2, and so forth.

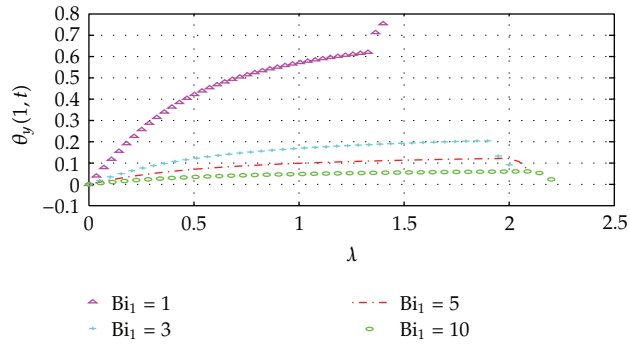

Figure 34: Effects of Bi_1 variation on the thermal criticality or blowup in the system.

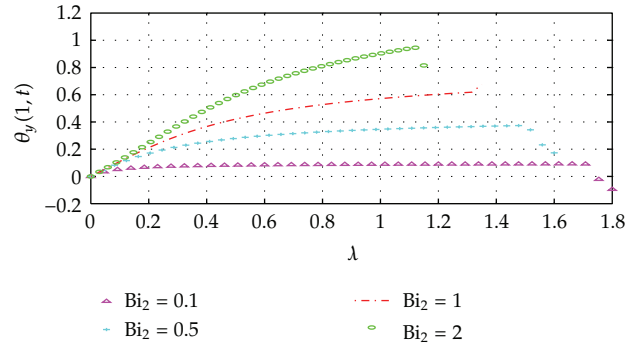

Figure 35: Effects of Bi_2 variation on the thermal criticality or blowup in the system.

5. Conclusion

We develop an unconditionally stable (works for any time step size) and convergent semi-implicit finite-difference scheme and utilize it to computationally investigate the transient dynamics of CO_2 emission, O_2 depletion, and thermal decomposition in a reacting slab. The solutions show that those processes that increase the oxidation reactions lead to enhanced oxygen depletion as well as increased carbon dioxide emission. The results also show that enhanced thermal stability and reduced carbon dioxide emission are best achieved by cutting down on those processes that would otherwise increase the oxidation reactions.

References

[1] J. Bebernes and D. Eberly, *Mathematical Problems from Combustion Theory*, vol. 83 of *Applied Mathematical Sciences*, Springer, New York, NY, USA, 1989.

[2] J. C. Quick and D. C. Glick, "Carbon dioxide from coal combustion: variation with rank of US coal," *Fuel*, vol. 79, no. 7, pp. 803–812, 2000.

[3] R. Betz and M. Sato, "Emissions trading: lessons learnt from the 1st phase of the EU ETS and prospects for the 2nd phase," *Climate Policy*, vol. 6, no. 4, pp. 351–359, 2006.

[4] R. Quadrelli and S. Peterson, "The energy-climate challenge: recent trends in GHG emissions from fuel combustion," *Energy Policy*, vol. 35, no. 11, pp. 5938–5952, 2007.

[5] J. M. Simmie, "Detailed chemical kinetic models for the combustion of hydrocarbon fuels," *Progress in Energy and Combustion Science*, vol. 29, no. 6, pp. 599–634, 2003.

[6] O. D. Makinde, "Exothermic explosions in a slab: a case study of series summation technique," *International Communications in Heat and Mass Transfer*, vol. 31, no. 8, pp. 1227–1231, 2004.
[7] E. Balakrishnan, A. Swift, and G. C. Wake, "Critical values for some non-class A geometries in thermal ignition theory," *Mathematical and Computer Modelling*, vol. 24, no. 8, pp. 1–10, 1996.
[8] S. Tanaka, F. Ayala, and J. C. Keck, "A reduced chemical kinetic model for HCCI combustion of primary reference fuels in a rapid compression machine," *Combustion and Flame*, vol. 133, no. 4, pp. 467–481, 2003.
[9] D. A. Frank-Kamenetskii, *Diffusion and Heat Transfer in Chemical Kinetics*, Plenum Press, New York, NY, USA, 1969.
[10] F. S. Dainton, *Chain Reaction: An Introduction*, Wiley, New York, NY, USA, 1960.
[11] R. vas Bhat, J. Kuipers, and G. Versteeg, "Mass transfer with complex chemical reaction in gasliquid system: two-steps reversible reactions with unit stoichiometric and kinetic orders," *Chemical Engineering Journal*, vol. 76, pp. 127–152, 2000.
[12] J. Warnatz, U. Maas, and R. Dibble, *Combustion: Physical and Chemical Fundamentals, Modeling and Simulation, Experiments, Pollutant Formation*, Springer and Co. K, Berlin, Hiedelberg GmbH, Germany, 2001.
[13] F. A. Williams, *Combustion Theory*, Benjamin & Cuminy Publishing, Menlo Park, Calif, USA, 2nd edition, 1985.
[14] M. A. Sadiq and J. H. Merkin, "Combustion in a porous material with reactant consumption: the role of the ambient temperature," *Mathematical and Computer Modelling*, vol. 20, no. 1, pp. 27–46, 1994.
[15] O. D. Makinde and T. Chinyoka, "Transient analysis of pollutant dispersion in a cylindrical pipe with a nonlinear waste discharge concentration," *Computers & Mathematics with Applications*, vol. 60, no. 3, pp. 642–652, 2010.
[16] O. D. Makinde and T. Chinyoka, "MHD transient flows and heat transfer of dusty fluid in a channel with variable physical properties and Navier slip condition," *Computers & Mathematics with Applications*, vol. 60, no. 3, pp. 660–669, 2010.
[17] T. Chinyoka, "Poiseuille flow of reactive Phan-Thien-Tanner liquids in 1D channel flow," *Journal of Heat Transfer*, vol. 132, no. 11, pp. 111701–7111708, 2010.
[18] T. Chinyoka, "Computational dynamics of a thermally decomposable viscoelastic lubricant under shear," *Journal of Fluids Engineering*, vol. 130, no. 12, pp. 1212011–1212017, 2008.